Journal of Applied Sciences 11 (9): 1544-1551, 2011
ISSN 1812-5654 / DOI: 10.3923/jas.2011.1544.1551

Drag Reduction of Biopolymer Flows

[1,2]A. Jaafar and [2]R.J. Poole
[1]Department of Mechanical Engineering, Universiti Teknologi Petronas, 31750 Tronoh, Perak, Malaysia
[2]Department of Engineering, University of Liverpool, Brownlow Street, Liverpool, L69 3GH, United Kingdom

Abstract: Drag reduction of rigid and semi-rigid biopolymers-scleroglucan (0.005 and 0.01% w/w) and xanthan gum (0.0124 and 0.07% w/w)-in a circular pipe and a concentric annular pipe (radius ratio $\kappa = 0.5$) have been investigated experimentally. The objective here is to assess and study the behaviour of these polymers and compare to the drag reduction by flexible polymers available in the literature. Pressure-drop, mean axial and complete Reynolds normal stress data measurements on the polymer solutions were conducted using laser Doppler anemometry. Measurements were also performed on the Newtonian solvent (water) for comparison. Rheological characterization of the polymers conducted over a wide range of concentrations (0.005-0.75% w/w) showed increased shear-thinning ability of the polymer solutions with increasing solution concentration. The pressure-drop measurements indicate that the effectiveness of these polymers as drag-reducing agents is only mildly dependent on the Reynolds number. Qualitative assessment of the turbulent peak values in the circular pipe flow shows behaviour resembling that of low drag-reducing (DR≤40%) flexible polymer solutions data available in the literature such as carboxymethylcellulose with increases in u'^{+} and decreases both in w'^{+} and v'^{+} generally when compared to that of the Newtonian flow at the same Reynolds number. The peak values of the turbulent fluctuation levels (normalized with U_B) in the annular pipe, however, shows a decreasing trend of the axial component below 40% drag reduction. Above this drag-reduction limit, the peak levels seemed to increase, generally, with drag reduction. Decrease in both w'/U_B and v'/U_B when compared to that of the Newtonian flow are observed at the same Reynolds number for all drag-reducing flows, similar to what is observed in the pipe-flow study.

Key words: Drag reduction, biopolymer, newtonian solvent, turbulent flow

INTRODUCTION

The phenomenon of drag reduction is seen as a reduction of pressure drop and skin friction in turbulent flow when polymer is added to the solvent, typically water. It has been the subject of extensive reviews by Virk (1975), Hoyt (1986), Graham (2004), White and Mungal (2008) and many others. A notional limit of 40% drag reduction has been set for pipe and channel flows, below which the flow is categorized as low drag-reducing and above which high drag-reducing (Warholic *et al*., 1999; Tiederman, 1990; Escudier *et al*., 2009). There are marked differences between these two categories. For low drag-reducing flows, the normalized mean velocity in law-of-the-wall form (u^+) remains parallel to the Newtonian data but is upshifted (Hoyt, 1986; Warholic *et al*., 1999; Tiederman, 1990; Escudier *et al*., 2009; Den Toonder *et al*., 1997; Ptasinski, 2002). In addition, the peak value of the normalized axial rms fluctuations (u'^{+}) increases, the peak values of the radial (v'^{+}) and tangential (w'^{+}) rms fluctuations decrease together with a monotonic decrease of the Reynolds shear stress ($\rho u'v'$) (Warholic *et al*., 1999; Tiederman, 1990; Ptasinski, 2002). Different trends are observed for high drag-reducing flows where there is a significant increase in the slope of the universal mean velocity profile (Warholic *et al*., 1999; Tiederman, 1990; Ptasinski, 2002). At such high levels of drag reduction the normalized axial rms fluctuation levels are ultimately suppressed with further suppression of the radial and tangential components. Concomitant decreases of the Reynolds shear stress to almost zero levels close to the maximum drag reduction asymptote (Virk, 1975) are observed with corresponding increases in the so-called polymer stress.

From these studies the behaviour of flexible polymer solutions as drag-reducing agents is now fairly well explored and understood. However, the drag-reducing mechanism of rigid or rod-like polymers has received considerably less attention partly because they appear not to be as effective at drag reducing at a given concentration as flexible polymer solutions (Paschkewitz *et al*., 2005). Microscopically, the difference

Corresponding Author: A. Jaafar, Department of Mechanical Engineering, Universiti Teknologi Petronas, 31750 Tronoh, Perak, Malaysia

between flexible polymer and rigid polymer is that prior to shearing, flexible polymer can be viewed as being in a randomly coiled configuration requiring some minimal value of shear rate to stretch the molecules, while a rigid polymer is already stretched in a rod-like conformation. Many biologically derived polymers are rigid or semi-rigid rod-like molecules (Tracy and Pecora, 1992) while all synthetic polymers are flexible polymer molecules (Doi and Edwards, 1986). Compared to flexible polymer solutions, rigid polymer solutions are more resistant to mechanical degradation (Paschkewitz *et al*., 2005). Scleroglucan and xanthan gum, as used in this study, are examples of rigid and semi-rigid biopolymers. These polymers are currently used as additives in the drilling fluids and also for polymer flooding of oil reservoirs (Stokke *et al*., 1992). They are environmentally and economically advantageous over oil-based drilling fluids and superior to water-based drilling fluids containing cellulosic and guar gum, for example, in terms of lubricating power and carrying capacity with the gelation property of scleroglucan reported to be better (Hamed and Belhadri, 2009).

MATERIALS AND METHODS

The measurements were carried out in a 23 m long circular pipe-flow facility as shown in Fig. 1. The test pipe comprised of 21 precision-bore borosilicate glass tubes, each of about 1029±2 mm long, a single glass tube 656 mm in length and one PVC plastic pipe, 1060 mm long, at the test-section entrance. The internal diameter of the tubes is 100.4±0.1 mm. A 5.81 m long annular-flow facility was also utilized as shown in Fig. 2. The test pipe comprised of four 1041 mm long, one 625 mm long and one 718 mm long precision-bore borosilicate glass tubes, with an average internal diameter of 100.4±0.1 mm and wall thickness of 5±0.1 mm. The inner centrebody was made of stainless steel thin walled tube with an outside diameter of 50.8 mm giving a radius ratio $\kappa = 0.506$ and a length-to-hydraulic diameter ratio of 117. The thin wall thickness of the centrebody gave a near neutral buoyancy in water based solution, minimizing hog and sag; i.e., the possibility of the centrebody to arch upwards or downwards is reduced. The centrebody was held in position by a thrust bearing located in the upstream end and a hydraulic jack tensioned to 3 tonnes axial load on the downstream end of the annulus.

A quantity of approximately 700 L of tap water was used as a solvent for the polymers. Prior to the addition of polymer, water was circulated within the facility to remove any dissolved air. Mixing of part of the solvent with the polymer powder was achieved by circulating the polymer solution within the mixing loop at a low pump speed for at least 5 h before the mixing loop was opened and the solution was circulated in the flow loop, allowing further mixing with the rest of the solvent in the pipe for at least

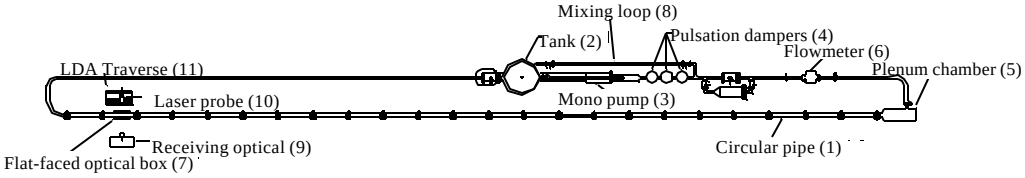

Fig. 1: Schematic diagram of the circular pipe-flow loop

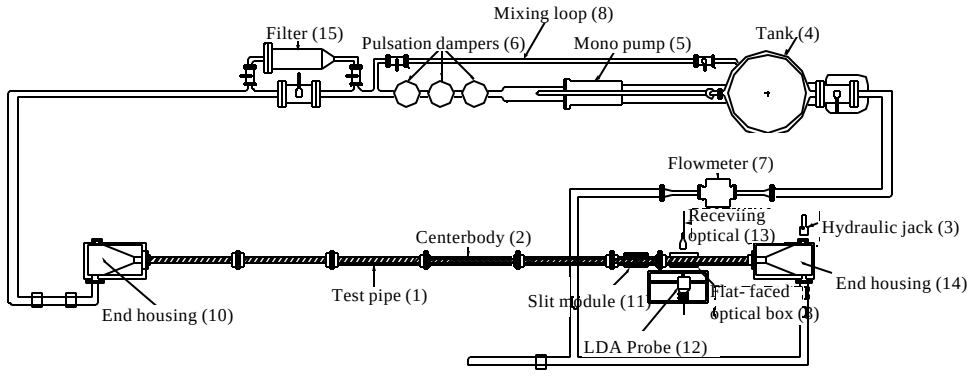

Fig. 2: Schematic diagram of the annular pipe-flow loop

another 5 h, until the solutions appeared to be visibly homogeneous. To retard bacteriological degradation of the solution, 37% (w/w) formaldehyde was added to the polymer solution at a concentration of 100 ppm. Seeding particles (Timiron MP-1005, mean diameter ≈5 μm supplied by S. Blanck Ltd.) were also added at a concentration of 1 ppm in order to increase the signal to noise ratio and the data rate for the Laser Doppler Anemometer (LDA) measurements. Measurements of fluid rheology for all the solutions were conducted prior to and after each LDA profile to check for signs of mechanical and bacteriological degradation where any decrease by more than 5% from the initial state was taken as a sign of degradation.

The fluid was driven from a 500 L capacity stainless steel tank by a positive displacement progressive cavity pump (Mono-type, E101 with a maximum flowrate of 0.025 m^3 sec^{-1}) with three pulsation dampers to reduce pulsations. A Coriolis mass flowmeter (Promass 63, manufactured by Endress + Hauser) was incorporated in the circular-pipe facility and a Fischer and Porter MAG-SM Series 1000 electromagnetic flowmeter (model 10D1) was incorporated in the annular-pipe facility. The temperature of the fluid was monitored using a platinum resistance thermometer positioned inside the tank with an accuracy of ±0.1°C.

The pressure drop was measured by means of a differential pressure transducer, GE Druck (LPX9381) with a range of 5000 Pa and an uncertainty of less than 1.5%, over a distance of 72D starting 140D downstream of the inlet for the circular pipe, where D is the diameter of the pipe. Pressure-drop measurements were conducted in the annular pipe at a location of $75.8D_H$ downstream of the inlet to the pipe test section over a distance of $41.3D_H$ where D_H ($\equiv D_o-D_i$) is the hydraulic diameter of the annulus with D_o and D_i being the diameter of the outer and inner pipes, respectively.

Mean velocity profiles and Reynolds normal stress measurements, i.e., u′, v′ and w′ were performed at a location 220D and $104.7D_H$ downstream of the inlet of the test section for the circular and annular-pipe flow, respectively using a Dantec Fiberflow LDA system with the aid of a flat faced optical box. The optical box is filled with water to minimize the amount of refractions of the beams making it possible to obtain data closer to outer pipe wall where refraction is the most due to the curved pipe wall. At each location across the annular gap, 10,000 to 30,000 data samples were collected and were processed using a simple ensemble-averaging method. A maximum statistical error, for a 95% confidence interval, was less than 0.5% in mean velocity and less than 1.5% in the turbulence intensity based on the method of (Yanta and Smith, 1973). The flowrates obtained from integration of the LDA mean velocity profiles were found to be within 1.5% of the values provided by the flowmeters.

WORKING FLUID CHARACTERIZATION

The scleroglucan (Actigum™ CS, provided by Cargill Incorporated and hereafter referred to as SG) used in this study is a non-ionic polysaccharide produced by the fungi of genus Sclerotium with a molecular weight reported by the supplier to be about 5.4×10^5 g mol^{-1}. Samples of Xanthan Gum (XG) were obtained from the Kelco Co. (Ketrol TF) with the molecular weight of an individual xanthan gum chain reported by the supplier to be in excess of 10^6 g mol^{-1}. Steady-shear measurements were conducted on small sample solutions (~500 mL) prepared separately outside the flow rigs over a wide range of concentrations for scleroglucan (0.005-0.5% w/w) and xanthan gum (0.01-0.75% w/w) at 20°C using a TA-Instruments Rheolyst AR 1000N controlled-stress rheometer. The measured viscometric data indicate increased shear thinning with concentration for both SG and XG.

PRESSURE-DROP MEASUREMENTS

The Fanning friction factor, f ($\equiv 2\tau_W/\rho U_B^2$) is plotted (in log-log coordinates) against the Reynolds number, Re ($\equiv \rho U_B D/\eta_W$) for water and scleroglucan in Fig. 3 for the circular pipe-flow study. Figure 4 shows the f-Re plot for water, sclerolgucan and xanthan gum in the annular-flow study. The Reynolds number is defined based on the bulk velocity, U_B, pipe diameter (or hydraulic diameter for the annulus) and the shear viscosity at the wall, η_W. The wall

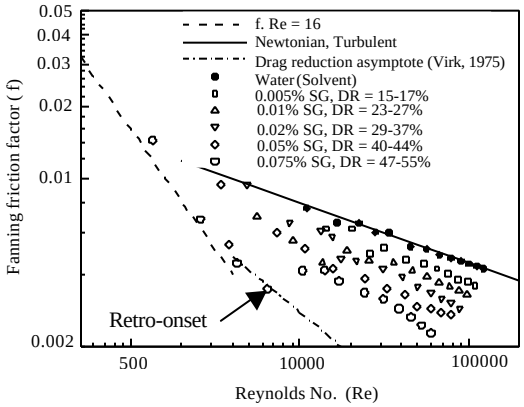

Fig. 3: f-Re data for various SG concentrations

shear viscosity was obtained from the Carreau-Yasuda model (Yasuda *et al*., 1981) fitted to the steady-shear viscosity data using the wall shear stress, τ_W, determined from the pressure-drop measurements.

In Fig. 3 the behaviour of water in the turbulent regime follows the empirical relationship for fully-developed turbulent pipe flow known as the Blasius approximation (Knudsen and Katz, 1958).

$$f = 0.0791Re^{-\frac{1}{4}} \quad (1)$$

The friction factors of scleroglucan solutions show increased deviation with increasing concentration from those of the Newtonian solvent (water) towards Virk's maximum drag reduction asymptote (Virk, 1975) given as:

$$f = 0.58Re^{-0.58} \quad (2)$$

These data exhibit ladder characteristics typical of Type B drag reduction as discussed by Virk *et al*. (1997), who initially proposed the idea of a distinction between flexible and rigid polymer drag reduction, where the friction factor variation with Reynolds number (plotted in log-log coordinates) is almost parallel to that of the Newtonian flow as the Reynolds number is increased. The f-Re data for 0.075% scleroglucan solution showed retro-onset (Virk *et al*., 1997) from the Virk's maximum drag reduction asymptote beyond which the friction factor increased and remained almost parallel to that of the Newtonian flow. The increase in friction factor is not a sign of degradation as the retro-onset is repeatable and within the experimental uncertainty.

In Fig. 4, an f-Re plot for water in the annular pipe, good agreement is observed with the empirical relationship given by Jones and Leung (1981) for radius ratio $\kappa = 0.5$.

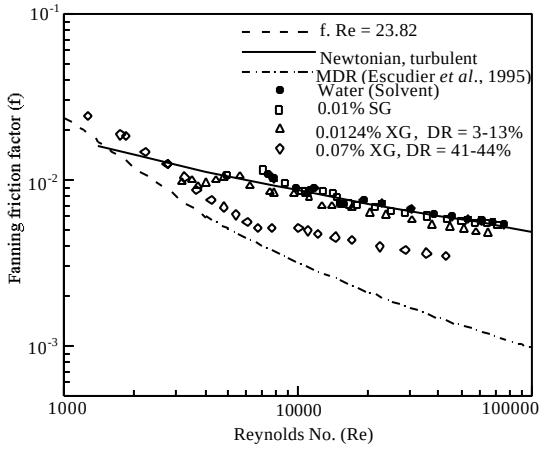

Fig. 4: f-Re data for SG and XG

$$\frac{1}{\sqrt{f}} = 4\log\left(1.343Re\, f^{1/2}\right) - 1.6 \quad (3)$$

within the high Reynolds number turbulent flow regime. The friction factor data within the turbulent regime is on average 14% higher than the data measured in the circular pipe at the same Reynolds number. The f-Re data for 0.01% scleroglucan is also shown in Fig. 4. The data clearly shows negligible amount of drag reduction where the friction factor values lie within the acceptable error of the Newtonian friction factor. These data shows lower drag-reducing ability of scleroglucan in the annular pipe compared to what is observed in the circular pipe. As the 0.01% scleroglucan solution did not show significant drag-reducing behaviour the drag reduction of a semi-rigid polymer, xanthan gum, at a concentration (c/c* where c* is the critical overlap concentration (Lapasin and Pricl, 1995) close to that of 0.01% scleroglucan is studied instead in an annular pipe, i.e., 0.0124% w/w xanthan gum is utilized. The f-Re data for 0.0124 and 0.07% xanthan gum shows an almost parallel deviation from the Newtonian data similar to what is observed for scleroglucan in the circular pipe flow.

The drag-reduction values quoted in Fig. 3 and 4 at several Reynolds numbers are calculated based on the friction factor of the polymer solution and the friction factor for water calculated at the same wall Reynolds number based on the Blasius approximation i.e.,

$$DR(\%) = \left[\frac{f_n - f_p}{f_n}\right] \times 100 \quad (4)$$

where, the subscripts n and p refer to the Newtonian fluid and the polymer solution, respectively.

MEAN AND RMS VELOCITY MEASUREMENTS

Mean axial velocity and complete Reynolds normal stress data, i.e., u', v' and w', were measured at several different Reynolds numbers, all in the turbulent-flow regime for both scleroglucan (0.005 and 0.01% w/w) and xanthan gum (0.0124 and 0.07% w/w). Control runs with a Newtonian fluid, water, also within the turbulent-flow regime at approximately identical Reynolds numbers were also performed as a basis for comparison.

The mean flow data for water in the circular pipe flow is shown in wall coordinates (i.e., u^+ ($\equiv u/u_\tau$) against y^+ ($\equiv \rho y u_\tau / \eta_W$) where ρ and y are the fluid density and the distance from the pipe wall, respectively) in Fig. 5. The term u_τ, the so called friction velocity as it has the dimensions of velocity, is given by:

$$u_\tau = \sqrt{\frac{\tau_W}{\rho}} \quad (5)$$

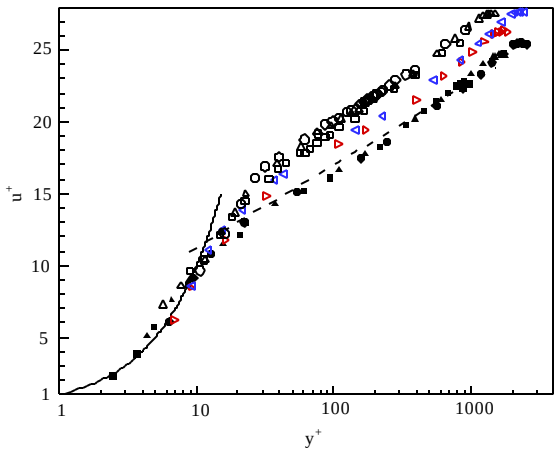

Fig. 5: Universal mean velocity distribution for water, 0.005 and 0.01% SG. ____: $u^+ = y^+$; - - -: $u^+ = 2.5 \ln y^+ + 5.5$; ■: Water, Re = 34000; ▲: Water, Re = 67000; •: Water, Re = 101000; ▷: 0.005% SG, Re = 65000, DR = 15%; ◁: 0.005% SG, Re = 109000, DR = 17%; □: 0.01% SG, Re = 36000, DR = 24%; Δ: 0.01% SG, Re = 67000, DR = 25%; ○: 0.01% SG, Re = 97000, DR = 27%

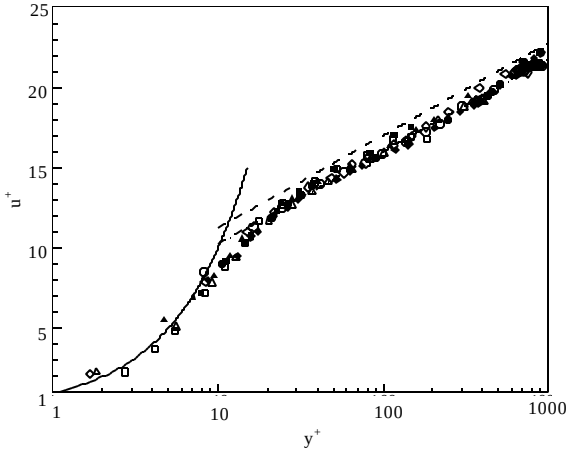

Fig. 6: Universal mean velocity distribution for water. ____: $u^+ = y^+$; - - -: $u^+ = 2.5 \ln y^+ + 5.5$; - · -: $u^+ = 2.5 \ln y^+ + 4.9$ (Clauser, 1956); □: Water (Inner), Re = 9900; ■: Water (Outer), Re = 9900; Δ: Water (Inner), Re = 30600; ▲: Water (Outer), Re = 30600; ◇: Water (Inner), Re = 61400; ◆: Water (Outer), Re = 61400; ○: Water (Inner), Re = 77000; •: Water (Outer), Re = 77000

For the Newtonian fluid good agreement is observed with the well-known log law (Tennekes and Lumley, 1972).

$$u^+ = 2.5 \ln y^+ + 5.5 \quad (6)$$

The data close to the wall are also in good agreement with that expected for the viscous sub layer (i.e., ($y^+ \leq 10$) $u^+ = y^+$). The scleroglucan data (shown in the same figure) in the viscous sublayer also follow $u^+ = y^+$ while in the Newtonian core region the data are shifted upward from but remain essentially parallel to the Newtonian data as expected for low drag-reducing flows (Warholic *et al.*, 1999; Escudier *et al.*, 2009).

Figure 6 shows the mean flow data of water in the annular pipe in wall coordinates. The friction velocity, u_τ is calculated using the wall shear stresses at the inner and outer walls. These wall shear stresses were calculated using the pressure-drop measurements data, $\Delta p/L$ and the zero shear stress location, $r_{\tau=0}$ (Knudsen and Katz, 1958) via

$$\tau_o = -\left(\frac{\Delta p}{L}\right)\left[\frac{R_o^2 - r_{\tau=0}^2}{2R_o}\right]$$
$$\tau_i = -\left(\frac{\Delta p}{L}\right)\left[\frac{r_{\tau=0}^2 - R_i^2}{2R_i}\right] \quad (7)$$

The location of zero shear stress has been determined to be within the experimental uncertainty from the location of maximum velocity by Japper-Jaafar *et al.* (2010) at a non-dimensional radial location ξ ($\equiv (r - R_i)/(R_o - R_i)$) of 0.44. As shown in the figure the data close to the walls are in good agreement with that expected for the viscous sublayer. In the Newtonian core region, the data for the inner and the outer walls collapse, in agreement with the empirical equation with the constant proposed by Clauser (1956):

$$u^+ = 2.5 \ln y^+ + 4.9 \quad (8)$$

as opposed to the well known log law constant in Eq. 6 which is applicable to circular pipe flows. Figure 7 shows the mean flow data in wall coordinates for 0.0124% xanthan gum. The xanthan gum data in the viscous sublayer follows $u^+ = y^+$ as expected. In the Newtonian core region, the data are shifted upward from but remained parallel to the Newtonian data. The higher values of u^+ are clear evidence of drag reduction. At the lowest measured Reynolds number, where the drag reduction is only about 3.2%, the outer wall data lie close to the Newtonian line and is only progressively upshifted with higher Reynolds number. Complete collapse of the inner and outer walls

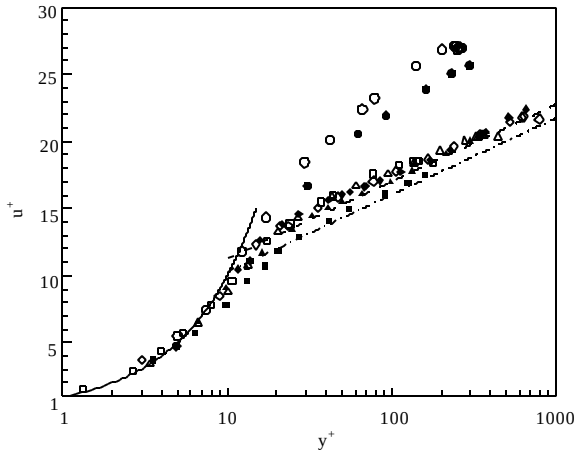

Fig. 7: Universal mean velocity distribution for 0.0124% XG. ____: $u^+ = y^+$; - - -: $u^+ = 2.5 \ln y^+ + 5.5$; - · -: $u^+ = 2.5 \ln y^+ + 4.9$ (Clauser, 1956); □: 0.0124% XG (Inner), Re = 10600, DR = 3.2%; ■: 0.0124% XG (Outer), Re = 10600, DR = 3.2%; Δ: 0.0124% XG (Inner), Re = 30300, DR = 10.3%; ▲: 0.0124% XG (Outer), Re = 30300, DR = 10.3%; ◇: 0.0124% XG (Inner), Re = 57600, DR = 11.6%; ◆: 0.0124% XG (Outer), Re = 57600, DR = 11.6%;): 0.07% XG (Inner), Re = 28700, DR = 42.3%; *: 0.07% XG (Outer), Re = 28700, DR = 42.3%

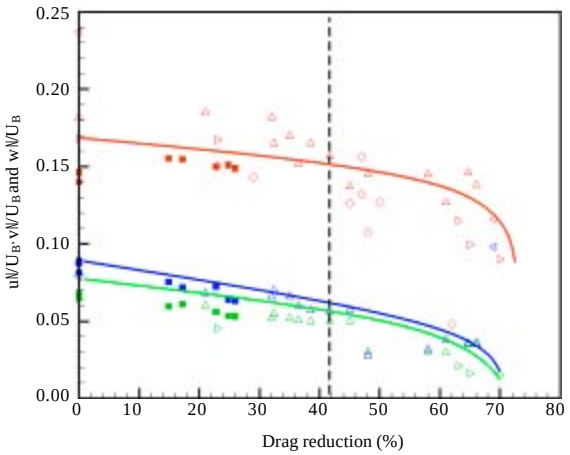

Fig. 8: Peaks of axial, radial and tangential fluctuation components normalized with the bulk velocity, U_B, against drag reduction (■: current study, Δ: PAA, XG, CMC (Presti, 2000), ▷: HPAM (Ptasinski *et al*., 2001), ◁: Macro Fibres (McComb and Chan, 1985), ◇: PEO, PAA (Allan *et al*., 1984), Red: u'/U_B, Green: v'/U_B, Blue: w'/U_B)

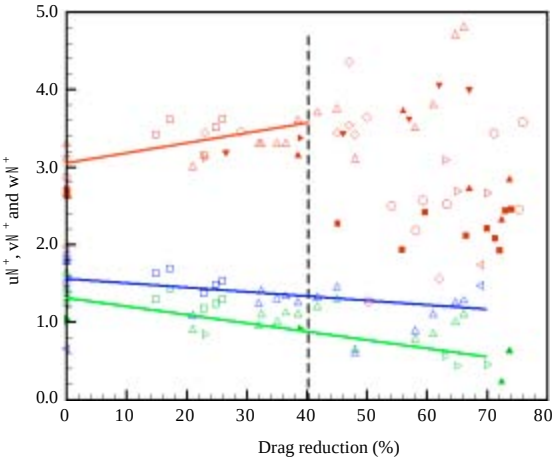

Fig. 9: Peaks of axial, radial and tangential fluctuation components in wall coordinates against drag reduction (□ :current study, Δ: PAA, XG, CMC (Presti, 2000), ▷: HPAM (Ptasinski *et al*., 2001), ◁: Macro Fibres (McComb and Chan, 1985), (◇: PEO, PAA (Allan *et al*., 1984), ○: PEO, PAA (Chung and Graebel, 1971), ■: PEO (Mizushina and Usui1977), ▲: PAA (Schummer and Thielen, 1980), ▼: PEO (McComb and Rabie, 1982), ►: PAA (Den Toonder *et al*., 1997), Red: u'^+, Green: v'^+, Blue: w'^+)

data only occurs at DR≈12%. These observations suggest that the initial contribution of drag reduction comes from the inner wall. At even higher levels of drag reduction, also shown in Fig. 7 for 0.07% xanthan gum measured at Re = 28700 where DR = 42.3%, both the inner and outer walls data are no longer parallel shifted from the Newtonian line, as expected for high drag-reducing flows (Warholic *et al*., 1999).

In Fig. 8, the peak values of the turbulent fluctuation components, normalized with the bulk velocity, have been plotted against drag reduction together with selected data from the literature for comparison (Den Toonder *et al*., 1997; Presti, 2000; Ptasinski *et al*., 2001; McComb and Chan, 1985; Allan *et al*., 1984; Chung and Graebel, 1971; Mizushina and Usui, 1977; Schummer and Thielen, 1980; McComb and Rabie, 1982). It can be seen that the data for the rigid rod-like polymer from the current study agree well with the trend of decreasing normalized peaks with increasing drag reduction similar to what is observed for two-dimensional channel flow (Escudier *et al*., 2009). In Fig. 9 the same data are plotted with the peak values normalized with the friction velocity, u_τ and the trend is for a decrease in the radial and tangential peak levels but

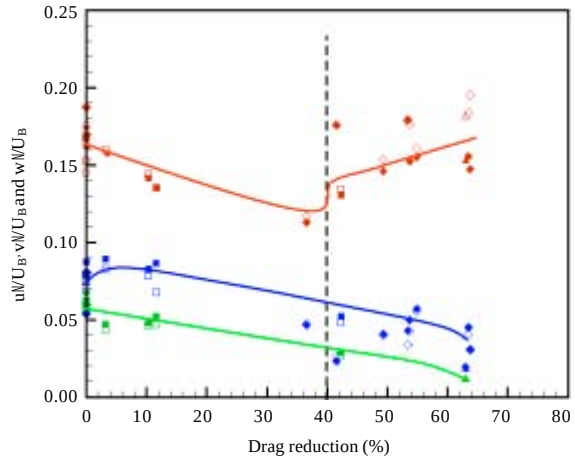

Fig. 10: Peaks of axial, radial and tangential fluctuation components normalized with the bulk velocity, U_B, against drag reduction (□ :current study, Δ: CMC (Nouri *et al*., 1993), ◇: (CMC, XG, LAPONITE/CMC (Escudier *et al*., 1995), Red: u'/U_B, Green: v'/U_B, Blue: w'/U_B, Hollow symbols: Inner wall, Filled symbols: Outer wall)

an increasing trend of axial peak level below 40% drag reduction with more complex behaviour at higher drag reduction.

In Fig. 10, the peak values of the turbulent fluctuation components close to the inner and outer walls, normalized with the bulk velocity, have been plotted against drag reduction together with the available data from the literature for the same annulus radius ratio of $\kappa = 0.5$ (Nouri *et al*., 1993; Escudier *et al*., 1995). The limited data for the semi-rigid polymer, xanthan gum, from the current study and the data obtained from the literature shows a decreasing trend below 40% drag reduction of the normalized axial peak level above which a slightly more complex but generally increasing trend is observed. The lines in the figures are included to guide the eye where clear trends are apparent. A dotted vertical line is also included within these figures to demarcate the two drag reduction regions. Apart from a slight increase of the normalized tangential component for DR≤12%, decreasing normalized radial and tangential components with drag reduction can also be seen from the data plotted. Due to limited information provided in the literature qualitative analysis of the wall data, i.e., peak values normalized with the friction velocity, u_τ, is not possible as was conducted for the pipe-flow studies.

CONCLUSIONS

The data presented here confirmed that rigid and semi-rigid rod-like polymer solutions, scleroglucan and xanthan gum, are effective as drag reducing agents in the circular and annular pipes with the drag-reduction effectiveness, which increases with solution concentration, found to be only mildly dependent on the Reynolds number. The results in the circular pipe-flow study show that the mean axial and turbulence structure data exhibit behavior typical of a low drag-reducing flexible polymer solution with increases in u'^+ and decreases both in w'^+ and v'^+ generally when compared to that of the Newtonian flow at the same Reynolds number. Qualitative analysis on the current limited peak values of the turbulent fluctuation levels (normalized with U_B) in the annular pipe indicated a different turbulent structure between the low and high drag-reducing annular flow than what is observed in the literature for pipe (Japper-Jaafar *et al*., 2009) and channel flows (Warholic *et al*., 1999). A decreasing trend below 40% drag reduction of the normalized axial peak level is seen above which a slightly more complex but generally increasing trend is observed instead.

REFERENCES

Allan, J.J., C.A. Greated and W.D. McComb, 1984. Laser doppler anemometer measurements of turbulent structure in non-Newtonian fluids. J. Phys. D Appl. Phys., 17: 533-549.

Chung, J.S. and W.P. Graebel, 1971. Laser anemometer measurements of turbulence in non-Newtonian pipe flows. Physics Fluids, 15: 546-554.

Clauser, F.H., 1956. The turbulent boundary layer. Adv. Applied Mech., 4: 1-51.

Den Toonder, J.M.J., M.A. Hulsen, G.D.C. Kuiken and F.T.M. Nieuwstadt, 1997. Drag reduction by polymer additives in a turbulent pipe flow: Laboratory and numerical experiments. J. Fluid Mech., 337: 193-231.

Doi, M. and S.F. Edwards, 1986. The Theory of Polymer Dynamics. Oxford Science Publications, Oxford, ISBN: 0-19-851976-1.

Escudier, M.P., I.W. Gouldson and D.M. Jones, 1995. Flow of shear-thinning fluids in a concentric annulus. Exp. Fluids, 18: 225-238.

Escudier, M.P., A.K. Nickson and R.J. Poole, 2009. Turbulent flow of viscoelastic shear-thinning liquids through a rectangular duct: Quantification of turbulence anisotropy. J. Non-Newtonian Fluid Mechanics, 160: 2-10.

Graham, M.D., 2004. Drag Reduction in Turbulent Flow of Polymer Solutions. In: Rheology Reviews, Binding, D.M. and K. Walters (Eds.). British Society of Rheology, New York, pp: 143-170.

Hamed, S.B. and M. Belhadri, 2009. Rheological properties of biopolymers drilling fluids. J. Petroleum Sci. Eng., 67: 84-90.

Hoyt, J.W., 1986. Drag Reduction, Encyclopaedia of Polymer Science and Engineering. Vol. 5, Wiley, New York, pp: 129-151.

Japper-Jaafar, A., M.P. Escudier and R.J. Poole, 2009. Turbulent pipe flow of a drag reducing, rigid rod-like polymer solution. J. Non-Newtonian Fluid Mech., 161: 86-93.

Japper-Jaafar, A., M.P. Escudier and R.J. Poole, 2010. Laminar, transition and turbulent annular flow of drag-reducing polymer solutions. J. Non-Newtonian Fluid Mech., 165: 1357-1372.

Jones, Jr. O.C. and J.C.M. Leung, 1981. An improvement in the calculation of turbulent friction in smooth concentric annuli. J. Fluids Eng., 103: 615-623.

Knudsen, J.G. and D.L. Katz, 1958. Fluid Dynamics and Heat Transfer. The McGraw-Hill Co., New York, ISBN: 0882759175.

Lapasin, R. and S. Pricl, 1995. Rheology of Industrial Polysaccharides: Theory and Applications. Blackie Academic and Professional, London, New York, ISBN: 0-7514-0211-7.

McComb, W.D. and L.H. Rabie, 1982. Local drag reduction due to injection of polymer-solutions into turbulent-flow in a pipe. 1. Dependence on local polymer concentration. AIChE J., 28: 547-557.

McComb, W.D. and K.T. Chan, 1985. Laser Doppler anemometer measurements of turbulent structure in drag reducing fibre suspensions. J. Fluid Mech., 152: 455-478.

Mizushina, T. and H. Usui, 1977. Reduction of eddy diffusion for momentum and heat in viscoelastic fluid flow in a circular tube. Physics Fluids, 20: s100-s108.

Nouri, J.M., H. Umur and J.H. Whitelaw, 1993. Flow of Newtonian and non-Newtonian fluids in concentric and eccentric annuli. J. Fluid Mech., 253: 617-641.

Paschkewitz, J.S., C.D. Dimitriropoulus, Y.X. Hou, V.S.R. Somandepalli, M.G. Mungal and P. Moin, 2005. An experimental and numerical investigation of drag reduction in a turbulent boundary layer using a rigid rodlike polymer. Physics Fluids, 17: 085101-0851017.

Presti, F., 2000. Investigation of transitional and turbulent pipe flow of non-Newtonian fluids. Ph.D. Thesis, University of Liverpool.

Ptasinski, P.K., F.T.M. Nieuwstadt, B.H.A.A. van Den Brule and M.A. Hulsen, 2001. Experiments in turbulent pipe flow with polymer additives at maximum drag reduction. Flow Turbulence Combustion, 66: 159-182.

Ptasinski, P.K., 2002. Turbulent flow of polymer solutions near maximum drag reduction: Experiments, simulations and mechanisms. Ph.D. Thesis, TU-Delft, The Netherlands.

Schummer, P. and W. Thielen, 1980. Structure of turbulence in viscoelastic fluids. Chem. Eng. Commun., 4: 593-606.

Stokke, B.T., A. Elgsaeter E.O. Bjornstad and T. Lund, 1992. Rheology of xanthan and scleroglucan in synthetic seawater. Carbohydrate Polymers, 17: 209-220.

Tennekes, H. and J.L. Lumley, 1972. A First Course in Turbulence. The MIT Press, Cambridge, Massachusetts, USA., ISBN: 978-0-262-20019-6.

Tiederman, W.G., 1990. The Effect of Dilute Polymer Solutions on Viscous Drag and Turbulence Structure. In: Structure of Turbulence and Drag Reduction, Gyr, A. (Ed.). Springer Verlag, Berlin, pp: 187-200.

Tracy, M.A. and R. Pecora, 1992. Dynamics of rigid and semirigid rodlike polymers. Annu. Rev. Phys. Chem., 43: 525-557.

Virk, P.S., 1975. Drag reduction fundamentals. AICHE. J., 21: 625-656.

Virk, P.S., D.C. Sherman and D.L. Wagger, 1997. Additive equivalence during turbulent drag reduction. AIChE J., 43: 3257-3259.

Warholic, M.D., H. Massah and T.J. Hanratty, 1999. Influence of drag-reducing polymers on turbulence: Effects of Reynolds number, concentration and mixing. Exp. Fluids, 27: 461-472.

White, C.M. and M.G. Mungal, 2008. Mechanics and prediction of turbulent drag reduction with polymer additives. Ann. Rev. Fluid Mech., 40: 235-256.

Yanta, W.J. and R.A. Smith, 1973. Measurements of turbulence-transport properties with a laser Doppler velocimeter. American Institute of Aeronautics and Astronautics, Aerospace Sciences Meeting, 11th, Washington, DC. USA., 10-12 Jan. 1973.

Yasuda, K., R.C. Armstrong and R.E. Cohen, 1981. Shear flow properties of concentrated solutions of linear and star branched polystyrenes. Rheol. Acta, 20: 163-178.